Quantitative assessment of pinning forces and magnetic penetration depth in NbN thin films from complementary magnetic force microscopy and transport measurements

T. Shapoval,[1,*] H. Stopfel,[1] S. Haindl,[1] J. Engelmann,[1] D. S. Inosov,[2] B. Holzapfel,[1] V. Neu,[1] and L. Schultz[1]
[1]*IFW Dresden, Institute for Metallic Materials, P. O. Box 270116, DE-01171 Dresden, Germany.*
[2]*Max Planck Institut für Festkörperforschung, Heisenbergstraße 1, DE-70569 Stuttgart, Germany*
(Received 21 January 2011; revised manuscript received 14 April 2011; published 15 June 2011)

Epitaxial niobium nitride thin films with a critical temperature of $T_c = 16$ K and a thickness of 100 nm were fabricated on MgO (100) substrates by pulsed laser deposition. Low-temperature magnetic-force-microscopy (MFM) images of the supercurrent vortices were measured after field cooling in a magnetic field of 3 mT at various temperatures. The temperature dependence of the penetration depth has been evaluated by a two-dimensional fitting of the vortex profiles in the monopole-monopole model. Its subsequent fit to a single s-wave-gap function results in the superconducting gap amplitude, $\Delta(0) = (2.9 \pm 0.4)$ meV = $(2.1 \pm 0.3)k_B T_c$, which perfectly agrees with the previous reports. The pinning force has been independently estimated from the local depinning of individual vortices by the lateral forces exerted by the MFM tip and from transport measurements. A good quantitative agreement between the two techniques shows that for low fields, $B \ll \mu_0 H_{c2}$, MFM is a powerful and reliable technique to probe the local variations of the pinning landscape. We also demonstrate that the monopole model can be successfully applied even for thin films with a thickness comparable to the penetration depth.

DOI: 10.1103/PhysRevB.83.214517 PACS number(s): 74.70.−b, 74.78.−w, 74.25.Wx, 68.37.Rt

I. INTRODUCTION

Vortex pinning is an important characteristic of type-II superconductors that allows tuning its properties without changing the chemical composition. Hence, the interpretation of pinning mechanisms,[1] the search for artificial defects with high pinning potentials,[2] and commensurable pinning effects by ordered arrays of defects[3–8] remain in the focus of basic research and application-based engineering. On the one hand, many high-power applications require materials with high pinning,[2] i.e., high critical-current density. On the other hand, logical applications (i.e., fluxonic devices[9]) benefit from low-pinning materials, which can be locally modified by introducing strong pinning sites in order to tune the dynamics of vortices and rectify their motion.[10]

A common way to investigate the pinning strength is to measure the sample response to an applied magnetic field (using magnetometry) or current (via transport measurements). These global methods probe the average value of the pinning force in a material as well as the collective dynamics of the elastic vortex lattice. However, the local modulations of the pinning landscape originating from different natural or artificial defects remain inaccessible to these techniques. This challenge can be addressed by local imaging methods, such as low-temperature magnetic force microscopy (LT-MFM), which is capable of correlating the superconducting (SC) vortex positions with the distribution of micro or nanostructural defects. It effectively combines the noninvasive imaging of flux lines with the ability to manipulate individual vortices by the stray field of the magnetic tip, offering a direct access to the local pinning force.[11] Nevertheless, reconciling the results of local and global measurements often represents a challenge.

In this paper, we will estimate the pinning forces in niobium nitride (NbN) thin films using two complementary methods. Local measurements by LT-MFM will be directly compared to transport measurements. Thin films of NbN have been chosen due to their high critical temperature, $T_c \approx 16$–17 K, that makes them suitable for LT-MFM studies in a wide temperature range. Moreover, this conventional superconductor has attracted attention due to its recent applications in sensitive SC bolometers.[12]

In contrast to the previous works,[13,14] where only the line profiles of the vortices were fitted, here we will evaluate the temperature dependence of the magnetic penetration depth, $\lambda(T)$, by performing a two-dimensional fit of the vortex profiles within the monopole-monopole model. Subsequently, we will use these values to estimate the SC energy gap of the NbN film, which we will compare to the direct tunneling measurements from the published literature.

II. EXPERIMENTAL DETAILS

Epitaxial NbN thin films with a thickness $d = 100$ nm were fabricated on single-crystalline MgO (100) substrates by pulsed laser deposition (PLD) using a Nb (99.95%) target in N_2 atmosphere with a pressure of 5×10^{-2} mbar. The base pressure in the chamber was 10^{-9} mbar. Prior to the film preparation, the Nb deposition rate was measured with an

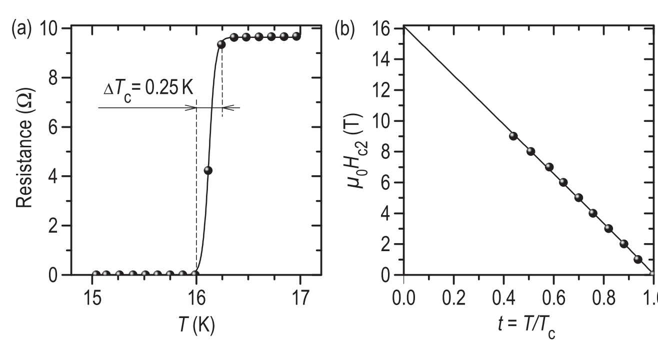

FIG. 1. (a) Zero-field resistive SC transition with a full width of $\Delta T_c \approx 0.25$ K. (b) Second critical field, $\mu_0 H_{c2}$, as a function of the reduced temperature, $t = T/T_c$. Points are the experimental values determined from transport measurements, whereas the solid lines are empirical fits.[15]

Inficon XTM/2 rate monitor. We used a KrF excimer laser (by Lambda-Physik) with a wavelength of 248 nm and a pulse duration of 25 ns. The substrates were heated up to 500 °C during deposition. Since the on-axis-PLD process leads to the formation of droplets on the surface, which pose a severe problem to the MFM scanning tip, a polishing technique[16] was applied to remove these obstacles providing a peak-to-valley roughness below 5 nm. X-ray diffraction patterns showed (00*l*) peaks (simple cubic structure) similar to previous reports.[17] The best samples exhibit a T_c (offset) at 16 K and a sharp resistive SC transition with a width $\Delta T_c \approx 0.25$ K [see Fig. 1(a)]. The temperature dependence of the second critical field, $\mu_0 H_{c2}$, determined from transport measurements, is shown in panel (b) of the same figure.

The LT-MFM measurements have been performed using a commercial scanning-probe microscope (by Omicron Cryogenic SFM).[18] We have used an MFM cantilever (Nanoworld MFMR) with characteristic force constant $k \approx 2.8$ N/m and a resonance frequency $f_0 \approx 80$ kHz. For the transport measurements, a 100-μm-wide bridge was structured by optical lithography and ion-beam etching. Transport measurements were performed in the standard four-point configuration using a 9 T physical property measurement system (PPMS) by Quantum Design.

III. MONOPOLE-MONOPOLE MODEL

The magnetic moment of the MFM tip (see the sketch in Fig. 2) can be well approximated to the first order by a magnetic monopole characterized by a "magnetic charge", $\tilde{m}$, located at a distance δ from the sharp end of the tip pyramid.[19,20] The field distribution from a single flux quantum, $\phi_0 = 2.07 \times 10^{-15}$ T m^2, measured just above the surface of the superconductor, is also similar to the magnetic field emanated by a magnetic monopole of $2\phi_0$, located at the depth $\lambda_{\mathrm{eff}} = p\lambda$ below the surface,[21] where λ is the magnetic penetration depth and p is a proportionality coefficient dependent on the film thickness. As demonstrated by Carneiro *et al.*,[21] this approximation perfectly works for bulk samples and thick films of $d > 4\lambda$. In this case, p varies from 1.0 at distances far above the surface ($z \gg \lambda$) to 1.27 in the vicinity of the surface ($z \ll \lambda$). For films of arbitrary thickness, the general solution for the field distribution also demonstrates the monopole-like character outside of the film. However, the prefactor p becomes an unknown parameter that could be accurately justified by solving the full field expression for the particular experimental conditions.[21] In the case of thin films, one should be careful using this simplified but very effective model. We will demonstrate in our work that application of the monopole model in the case of thin films with a thickness comparable to the penetration depth allows proper assessment of λ from MFM vortex imaging.

With these assumptions, the magnetic induction of the vortex, $\mathbf{B}(\mathbf{r},z)$, taken at a distance z above the surface, can be approximated by

$$\mathbf{B}(\mathbf{r},z) = \frac{\phi_0}{2\pi}\frac{(\mathbf{r}-\mathbf{r}_0)+(z+p\lambda)\,\mathbf{e}_z}{[(\mathbf{r}-\mathbf{r}_0)^2+(z+p\lambda)^2]^{3/2}}, \tag{1}$$

where $\mathbf{e}_z$ is the unit vector perpendicular to the film, $\mathbf{r}_0$ is the position of the vortex core, and $\mathbf{r}$ is the radial distance from its center. This leads us to the tip-vortex-interaction force, $\mathbf{F}(\mathbf{r},z)$, in the monopole-monopole model

$$\mathbf{F}(\mathbf{r},z) = \tilde{m}\mathbf{B}(\mathbf{r},z). \tag{2}$$

Taking into account that the shift of the resonance frequency of the cantilever measured by MFM, Δf, is proportional to the z derivative of the normal component of the force that acts between the tip and the sample,[19,20,22] $\partial_z F_z(\mathbf{r},z)$, we obtain the following expression for the measured signal:

$$\Delta f = -\frac{f_0}{2k}\frac{\tilde{m}\phi_0}{2\pi}\frac{(\mathbf{r}-\mathbf{r}_0)^2-2(z+p\lambda+\delta)^2}{[(\mathbf{r}-\mathbf{r}_0)^2+(z+p\lambda+\delta)^2]^{5/2}}. \tag{3}$$

As the magnetic induction of the vortex is maximal at the center and decays rapidly with r, the strongest interaction in z direction between the tip and the vortex occurs when the tip passes the center of the vortex. Thus the maximal z component of this force is reached at $r = r_0$,

$$\max(F_z)_{r=r_0} = \frac{\tilde{m}\phi_0}{2\pi}\frac{1}{(z+p\lambda+\delta)^2}. \tag{4}$$

The benefit of the monopole-monopole model is that all spatial parameters of the problem (z, λ_{eff}, and δ) enter Eqs. (3) and (4) additively, hence, the sum in the denominator can be redefined as an effective tip-sample distance

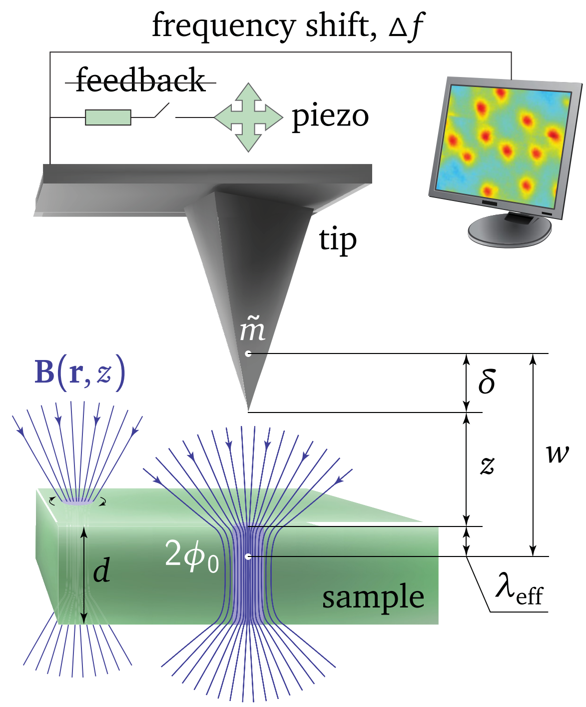

FIG. 2. (Color online) A schematic representation of the MFM imaging procedure and an illustration of the monopole-monopole model. The magnetized MFM tip, driven by a piezo element, scans above the surface of the sample at a given distance, z. During measurement, the feedback loop, which is typically used to stabilize the resonance frequency of the tip during topographic imaging, is deactivated. One measures a shift of the resonance frequency, Δf, induced by the magnetic field of the vortices, $\mathbf{B}(\mathbf{r},z)$. In the monopole-monopole model, described in the text, both the tip and the vortex are approximated by magnetic monopoles at distances $z+\delta$ and λ_{eff} from the surface of the sample, respectively.

$w = z + \lambda_{\text{eff}} + \delta$. It represents the distance between imaginary magnetic monopoles within the tip and the vortex, as illustrated by the white dots in Fig. 2.

The ratio between the lateral and vertical forces that act during scanning typically varies from 0.3 for a tip with a less sharp pyramid[23] to $2/(3\sqrt{3}) \approx 0.38$ for the monopole-monopole model.[11,23] This results in the following maximum lateral component of the tip-vortex-interaction force:

$$\max(F_{\text{lat}}) \approx 0.38 \max(F_z). \tag{5}$$

Obviously, noninvasive imaging of vortices by MFM is possible only as long as the vortices are pinned. The tip-vortex-interaction force can be accurately tuned during scanning by varying the tip-sample separation, z.[11] If this force exceeds the pinning force of an individual vortex at a natural or artificial defect, the vortex can be dragged away from its initial position. Likewise, if the tip-sample distance is kept constant, an increase in temperature can lead to the local depinning of individual flux lines during scanning due to the temperature dependence of the pinning force.

IV. LOCAL DEPINNING OF INDIVIDUAL FLUX LINES

We have mapped the temperature dependence of the vortex distribution after field cooling the sample to ~8 K in a vertical applied magnetic field of $\mu_0 H_z = -3$ mT (Fig. 3) and, subsequently, increasing the temperature in steps of 2 K. The tip-sample distance was kept constant at $z = 30$ nm, so that Eq. (4) can be applied. The negative direction of the field corresponds to the magnetic repulsion between the MFM tip and the vortex, and therefore the vortices appear as red (dark grey) objects in the false-color images presented in Fig. 3. In all panels, the white circles depict the positions of the vortex cores at a base temperature to emphasize the tip-induced changes in their position as the temperature is increased. These positions were determined by a two-dimensional (2D) fitting procedure[24] applied to the regions indicated by rectangles. The benefit of this method is that, in principle, it allows for a subpixel resolution of the fitting, given that the noise in the measured data is sufficiently low.

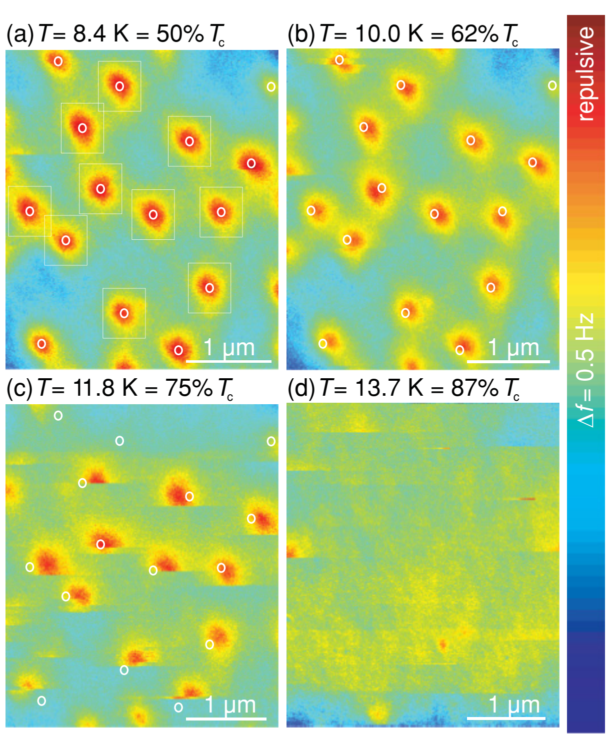

FIG. 3. (Color online) Vortex images measured at a distance $z = 30$ nm from the surface of a NbN film after field cooling in -3 mT at various temperatures: (a) 50%, (b) 62%, (c) 75%, and (d) 87% T_c. The slow-scanning direction is top to bottom. Depinning of vortices by the magnetic tip can be seen in panels (c) and (d).

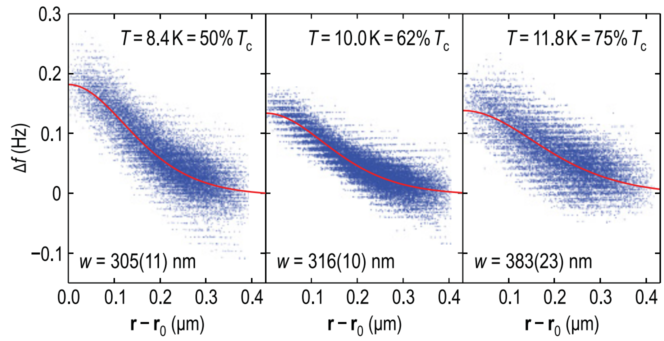

FIG. 4. (Color online) Temperature dependence of the averaged vortex profile. Blue points are the measured signal, solid lines are least-squares fits to the monopole-monopole model.

At temperatures not exceeding ~50%T_c [see Fig. 3], noninvasive imaging of vortices takes place, indicating that the pinning exceeds the lateral thrust of the MFM tip. Statistical image analysis, such as described by Inosov *et al.*,[24] reveals that the vortices form a highly disordered hexagonal lattice due to the pinning by natural defects.

At higher temperatures, the decreasing contrast of the vortex profile signifies a natural increase in the penetration depth, λ, that characterizes the decay of the magnetic field outside of the vortex core. At 62% T_c [see Fig. 3(b)], most vortices are still in their original positions, implying that the tip-vortex-interaction force is still lower than the typical pinning force of a single vortex. Only 2 out of 14 vortices, visualized in the figure, have been irreversibly dragged away from their initial positions (depicted as white circles) to the nearest pinning sites with higher pinning potentials. This indicates the existence of a slightly modulated pinning landscape in the NbN film and, hence, a spatial variation of the pinning force, as expected for natural defects.

At 75% T_c [see Fig. 3(c)], the movement of nearly every vortex by the MFM tip can be seen. Indeed, because most vortices are irreversibly dragged away by the tip as it passes close to the core, moved vortices appear half-cut in the image. Consequently, at this temperature the pinning force for the majority of the vortices is equal to the maximal lateral force exerted by the MFM tip onto the vortex, see Eq. (5). Only one vortex at the bottom-right part of the image remains stable evidencing the locally enhanced pinning force at this position. On the other hand, three other vortices are fully dragged away as soon as the tip starts crossing their field lines. At even higher temperatures [see Fig. 3(d)], vortices can no longer be imaged.

TABLE I. Temperature dependence of the effective tip-sample distance in the monopole-monopole model, $w = z + p\lambda + \delta$, the fitted peak amplitude from Fig. 4, $\Delta f(\mathbf{r} = \mathbf{r}_0)$, and the corresponding lateral tip-vortex interaction, max(F_{lat}).

Temperature (K)	8.4	9.1	10.0	11.8
w (nm)	305(11)	308(10)	316(10)	383(23)
$\Delta f(\mathbf{r} = \mathbf{r}_0)$ (Hz)	0.182(4)		0.134(3)	0.138(6)
max(F_{lat}) (pN)	0.74(3)		0.56(2)	0.70(5)

Here, the vortices are being continuously dragged by the tip during scanning.

For a quantitative analysis of the vortex profiles, their core positions, $\mathbf{r}_0$, were first determined using 2D fitting. To gather sufficient statistics for the application of the monopole-monopole model, the signal Δf from within the neighborhood of every vortex [white rectangles in Fig. 3(a)] has been plotted versus $|\mathbf{r} - \mathbf{r}_0|$, as shown in Fig. 4. In this figure, every data point corresponds to a pixel in the original MFM image, whereas data points originating from different vortices are combined in one plot. The resulting clusters of points ($\sim$ 16 000 points per image) can be fitted to Eq. (3) (solid lines) in order to obtain the average value of $w = z + p\lambda + \delta$ for every temperature with a sufficiently small statistical error. The results of these fits are summarized in Table I.

V. LOCAL PINNING FORCES AND THE PENETRATION DEPTH

Now we can proceed to the quantitative estimation of the pinning force. Combining Eqs. (3)–(5), we obtain

$$\max(F_{\mathrm{lat}}) \approx 0.38\,\frac{kw}{f_0}\,\Delta f(\mathbf{r} = \mathbf{r}_0). \tag{6}$$

Substituting the fitting results from Fig. 4 and the known parameters of the tip into this expression, we can calculate the temperature-dependent lateral tip-vortex forces that are listed in Table I with an average value of 0.67 ± 0.09 pN.[28] Since we already know that the local pinning force decreases sufficiently to allow depinning of most vortices at $T \approx 12$ K $= 75\%\ T_c$, we can use the calculated value as an estimate of the mean local pinning force at this temperature:

$$F_{\mathrm{p}}(T = 12\,\mathrm{K}) \approx (0.67 \pm 0.09)\,\mathrm{pN}. \tag{7}$$

The results of the same fit also provide a local probe for the temperature-dependent penetration depth,[13,14,26,27,29] in our case given by

$$\lambda(T) \approx [w(T) - z - \delta]/p. \tag{8}$$

The temperature-independent parameter $z \ll \lambda$ is fixed during measurement and it is known, so it can be easily subtracted, whereas $\lambda_{\mathrm{eff}}(T) = p\lambda(T)$ and δ are generally unknown and need to be determined. In Fig. 5, we have plotted the measured $[w(T) - z]/p$ value, assuming $p = 1.27$, which corresponds to the theoretical prediction for a thick film. According to Eq. (8), this value equals to $\lambda(T) + \delta/p$, and therefore represents an upper estimate for the actual penetration depth. The parameter δ, being a property of the tip and depending both on the temperature and the stray field of the sample, usually has

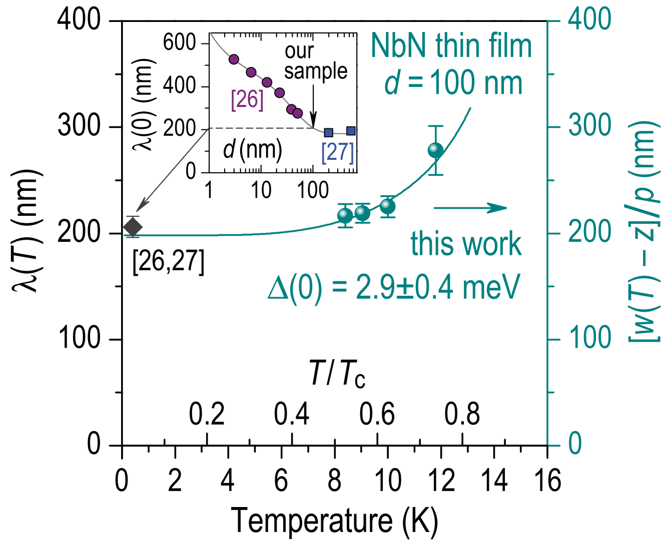

FIG. 5. (Color online) Temperature dependence of the $[w(T) - z]/p$ values for $p = 1.27$ (plotted on the right axis) in comparison to $\lambda(0)$ (left axis). The solid line is a fit to an empirical model with a single s-wave gap.[25] The value of $\lambda(0)$ for our film thickness was obtained by an interpolation of the d-dependent literature data,[26,27] as shown in the inset. The solid grey line is an empirical fit. A good agreement of our results with the published value indicates that the δ/p correction is negligible in our case.

a large uncertainty and requires a special calibration of the tip in order to be determined.[20,30] In the general case, it may lead to a non-negligible constant offset of the measured penetration depth from its true value. In such a case, δ would have to be considered as a free parameter of the model. However, in the special case when $\delta/p \ll \lambda$, this correction can be neglected. To quantify the δ/p correction in the present work, we resorted to a comparison of our temperature-dependent data (represented by spheres in Fig. 5) to the low-temperature value $\lambda(0) \approx 205$ nm (dark gray diamond in Fig. 5). The latter has been obtained by interpolating the directly measured $\lambda(0)$ values from the literature for different film thicknesses,[26,27] as shown in the inset of Fig. 5, and taking the intermediate value at $d = 100$ nm. The fact that the lowest-temperature data point from our MFM measurement nearly coincides (within the statistical error) with this reference value of $\lambda(0)$ indicates that the δ/p correction is negligible in our case. If this was not the case, the application of a 2D geometrical model of the tip[14] could be used to estimate the unknown tip parameter. However, it would simultaneously increase the uncertainty in the extracted quantitative values. The next step to a better quantitative interpretation of the MFM data would be the systematic precharacterization of the MFM tip for the exact determination of the tip parameters (i.e, monopole moment and monopole distance).

Now, let us discuss the more general case of $p \neq 1.27$, which could occur for thin films. At large distances from the sample, where the dipolar moment gives the dominant contribution to the stray-field distribution, p is expected to grow monotonically as $\coth(d/2\lambda)$ with decreasing film thickness.[21] However, in the limit of smaller distances ($z/\lambda \ll 1$) in which our MFM measurements are performed, higher-order multipole contributions can no longer be neglected, hence, a similar analytical expression no longer exists. An analysis of the calculations, presented in Fig. 2(a) in Ref. 21, for our case of $d/\lambda = 0.5$ indicates that in the immediate vicinity of the film, p does not deviate from the bulk limit as substantially as at large distances. This can also be concluded from our Fig. 5; a substantially higher value of p would reduce the plotted values below the lower limit given by the reference value $\lambda(0)$. Therefore, we can conclude that the agreement between our lowest-temperature MFM data point and $\lambda(0)$ indicates that no deviations from the $p = 1.27$ limit are observable within our experimental uncertainty.

An independent test for the validity of our approximations is also obtained by fitting the temperature dependence of the penetration depth. The solid line in Fig. 5 is an empirical fit to the formula of Evtushinsky *et al.*,[25] which gives an analytical relationship between $\lambda(T)$ and the SC gap $\Delta(0)$. For a conventional superconductor with a single isotropic s-wave gap, it becomes

$$\lambda(T) = \lambda(0)\left[1 - M\left(\frac{\Delta(T)}{k_B T}\right)\right]^{-1/2}, \tag{9}$$

where $\lambda(0)$ depends only on the band structure, whereas all the temperature-dependent quasiparticle effects are included in the approximant function[25]

$$M(t) = 4\,(e^{t/2} + e^{-t/2})^{-2}\sqrt{\pi t/8 + 1/(1+\pi t/8)}. \tag{10}$$

The temperature dependence of the SC gap in Eq. (9) is approximated by[31]

$$\Delta(T) = \Delta_0 \tanh\left(\frac{\pi}{2}\sqrt{T_c/T - 1}\right). \tag{11}$$

The resulting fit yields a value of $\Delta(0) = (2.9 \pm 0.4)$ meV $=$ $(2.1 \pm 0.3)k_B T_c$, which perfectly agrees with direct tunneling measurements[26,27] and is slightly above the weak-coupling limit of $1.76 k_B T_c$ predicted by the Bardeen-Cooper-Schrieffer (BCS) theory.[32] Such an agreement can not be accidental; it confirms the validity of the described procedure for the quantitative determination of $\lambda(T)$ from the MFM data on thin films with a thickness comparable to the penetration depth.

It is useful to note that an arbitrary value of p does not add a new fitting parameter to the model, as it can be absorbed into $\lambda_{\mathrm{eff}}(0) = p\lambda(0)$. Then, Eqs. (8) and (9) can be combined into the fitting formula

$$w(T) - z = \lambda_{\mathrm{eff}}(0)\left[1 - M\left(\frac{\Delta(T)}{k_B T}\right)\right]^{-1/2} + \delta$$

with three independent parameters: $\lambda_{\mathrm{eff}}(0)$, $\Delta(0)$, and δ.

VI. GLOBAL ESTIMATE OF THE PINNING FORCES

While MFM provides access to the pinning force of individual vortices, global characterization methods, such as transport or magnetization measurements, explore the collective behavior of the flux-line lattice. They evaluate the mean pinning force within the whole sample volume, considering also the elastic interaction between individual flux lines as well as the collective pinning.[15] For small magnetic fields, $B \ll \mu_0 H_{c2}$, the distance between vortices is larger than

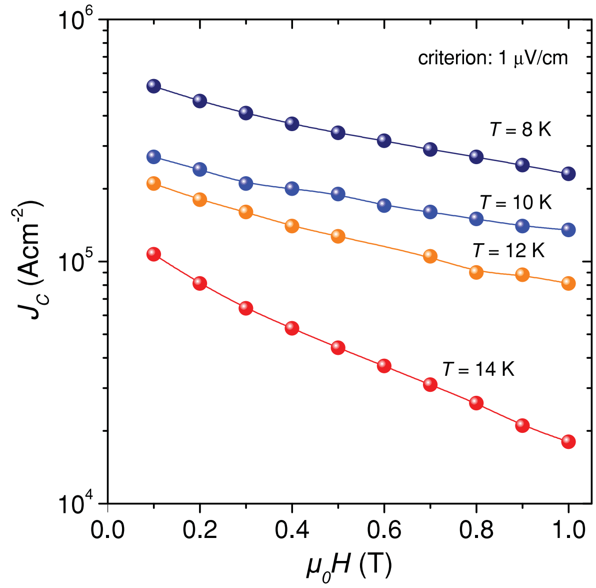

FIG. 6. (Color online) Dependence of the critical current density, J_c, on the applied magnetic field for different temperatures: 8, 10, 12, and 14 K.

λ. Such vortices can be treated as independent noninteracting objects. In this limit, collective effects can be ignored and the pinning force per vortex can be calculated as F_p^g/N, where F_p^g is the average pinning force and N is the number of vortices within the sample surface.

The pinning force is equal to the maximal sustainable Lorentz force that does not move vortices while the current flows,[15]

$$F_p^g(B) = V J_c B = S d J_c B, \tag{12}$$

where J_c is the critical current density, S is the surface area of the sample, and d is the sample thickness. The number of vortices is $N = BS/\phi_0$, hence, the pinning force per vortex is

$$F_p^g/N = J_c d\phi_0. \tag{13}$$

The dependence of J_c on the applied magnetic field for temperatures between 8 and 14 K is presented in Fig. 6. The resulting temperature dependence of the pinning force per vortex, F_p^g/N, calculated from these $J_c(H)$ curves, is given in Table II. One can immediately appreciate the agreement between the value of $F_p^g/N = 0.62$ pN that resulted from the transport measurements at $T = 12$ K with that of (0.67 ± 0.09) pN that we extracted earlier from the MFM data at a similar temperature. Taking into account that the pinning force varies by nearly a factor of five in the studied temperature range,

TABLE II. Critical current density and average pinning force per vortex at different temperatures, evaluated from the transport data in Fig. 6, for $B = 0$.

Temperature (K)	8	10	12	14
J_c (10^5 A/cm^2)	10	5	3	2
F_p^g/N (pN)	2.07	1.04	0.62	0.42

such an agreement, within 8% between local and global measurements, is indeed remarkable.

VII. SUMMARY

To conclude, we found perfect agreement between the values of the pinning force per vortex estimated from the local depinning of individual vortices by the MFM tip and globally from the critical current measurements. We demonstrated that for low fields, $B \ll \mu_0 H_{c2}$, MFM is a powerful and reliable method to probe the local space variation of the pinning landscape. The monopole-monopole model, originally derived for $d > 4\lambda$,[21] proved to be successful even for thin films with a thickness comparable to the penetration depth. With this knowledge, the quality of such very thin films, which are actually employed for the application in SC bolometers,[12] can be perfectly analyzed using magnetic force microscopy.

Finally, we used accurate 2D fitting of the vortex profiles to extract the London penetration depth of the NbN film and the SC energy gap. The statistical errors of this method are small enough to ensure that the extracted gap $\Delta(0) = (2.9 \pm 0.4)$ meV agrees with the directly measured values.[26,27] Although similar methods of extracting the gap amplitude from the muon-spin rotation (μSR), small-angle neutron scattering (SANS), microwave surface-impedance (MSI), or magnetization measurements of the temperature-dependent penetration depth are well developed,[33] their application to the analysis of temperature-dependent LT-MFM images is only becoming a standard practice.[29]

Based on the agreement of the extracted penetration depth, SC gap, and the local pinning force with those measured directly by complementary methods, we can conclude that the monopole model remains valid for practical purposes in our case of a thin film with $d/\lambda \approx 0.5$.

ACKNOWLEDGMENTS

We are grateful to E. H. Brandt and S. Vock for fruitful discussions, to K. Osse, S. Sieber, and I. Mönch for sample preparation, to D. Meier and M. Gründlich for technical assistance in sample polishing, to U. Wolff for MFM tip preparation, and to Kawia Scharle for the design of Fig. 2.

*t.shapoval@ifw-dresden.de

[1] G. Blatter, M. V. Feigelman, V. B. Geshkenbein, A. I. Larkin, and V. M. Vinokur, Rev. Mod. Phys. **66**, 1125 (1994).

[2] S. R. Foltyn, L. Civale, J. L. Manus-Driscoll, Q. X. Jia, B. Maiorov, H. Wang, and M. Maley, Nat. Mater. **6**, 631 (2007).

[3] V. V. Moshchalkov, M. Baert, V. V. Metlushko, E. Rosseel, M. J. Van Bael, K. Temst, R. Jonckheere, and Y. Bruynseraede, Phys. Rev. B **54**, 7385 (1996).

[4] A. Bezryadin, Yu. N. Ovchinnikov, and B. Pannetier, Phys. Rev. B **53**, 8553 (1996); V. Metlushko, U. Welp, G. W. Crabtree, Z. Zhang, S. R. J. Brueck, B. Watkins, L. E. DeLong, B. Ilic, K. Chung, and P. J. Hesketh, *ibid.* **59**, 603 (1999); V. V. Moshchalkov, M. Baert, V. V. Metlushko, E. Rosseel, M. J. Van Bael, K. Temst, Y. Bruynseraede, and R. Jonckheere, *ibid.* **57**, 3615 (1998); C. Reichhardt, C. J. Olson, and F. Nori, *ibid.* **57**, 7937 (1998); Phys. Rev. Lett. **78**, 2648 (1997); S. B. Field, S. S. James, J. Barentine, V. Metlushko, G. Crabtree, H. Shtrikman, B. Ilic, and S. R. J. Brueck, *ibid.* **88**, 067003 (2002); M. Baert, V. V. Metlushko, R. Jonckheere, V. V. Moshchalkov, and Y. Bruynseraede, *ibid.* **74**, 3269 (1995); Z. Jiang *et al.*, Appl. Phys. Lett. **84**, 5371 (2004); A. A. Zhukov *et al.*, *ibid.* **83**, 4217 (2003).

[5] A. Yu. Aladyshkin, A. V. Silhanek, W. Gillijns, and V. V. Moshchalkov, Supercond. Sci. Technol. **22**, 053001 (2009).

[6] J. I. Martin, M. Velez, J. Nogues, and Ivan K. Schuller, Phys. Rev. Lett. **79**, 1929 (1997); D. J. Morgan and J. B. Ketterson, *ibid.* **80**, 3614 (1998); M. J. Van Bael, J. Bekaert, K. Temst, L. Van Look, V. V. Moshchalkov, Y. Bruynseraede, G. D. Howells, A. N. Grigorenko, S. J. Bending, and G. Borghs, *ibid.* **86**, 155 (2001); J. E. Villegas, C. P. Li, and I. K. Schuller, *ibid.* **99**, 227001 (2007); J. E. Villegas *et al.*, Science **302**, 1188 (2003); Y. Jaccard, J. I. Martin, M.-C. Cyrille, M. Véelez, J. L. Vicent, and I. K. Schuller, Phys. Rev. B **58**, 8232 (1998); S. Erdin, A. F. Kayali, I. F. Lyuksyutov, and V. L. Pokrovsky, *ibid.* **66**, 014414 (2002); M. J. Van Bael, M. Lange, S. Raedts, V. V. Moshchalkov, A. N. Grigorenko, and S. J. Bending, *ibid.* **68**, 014509 (2003); A. V. Silhanek *et al.*, Appl. Phys. Lett. **89**, 182505 (2006); **90**, 182501 (2007); S. Haindl *et al.*, Supercond. Sci. Technol. **21**, 045017 (2008).

[7] A. Hoffmann, L. Fumagalli, N. Jahedi, J. C. Sautner, J. E. Pearson, G. Mihajlović, and V. Metlushko, Phys. Rev. B **77**, 060506 (2008).

[8] T. Shapoval, V. Metlushko, M. Wolf, B. Holzapfel, V. Neu, and L. Schultz, Phys. Rev. B **81**, 092505 (2010).

[9] B. Y. Zhu, F. Marchesoni, and F. Nori, Phys. Rev. Lett. **92**, 180602 (2004).

[10] C. C. de Souza Silva, A. V. Silhanek, J. Van de Vondel, W. Gillijns, V. Metlushko, B. Ilic, and V. V. Moshchalkov, Phys. Rev. Lett. **98**, 117005 (2007); G. Carneiro, Physica C **432**, 206 (2005).

[11] E. W. J. Straver *et al.*, Appl. Phys. Lett. **93**, 172514 (2008); O. M. Auslaender *et al.*, Nat. Phys. **5**, 35 (2009); T. Shapoval *et al.*, Physica C **470**, 867 (2010).

[12] A. D. Semenov *et al.*, Appl. Phys. Lett. **87**, 173508 (2005);
S. Cherednichenko *et al.*, Rev. Sci. Instrum. **79**, 034501 (2008); F. Sizov, Opto-Electron. Rev. **18**, 10 (2010).

[13] M. Roseman and P. Grütter, New J. Phys. **3**, 24.1 (2001).

[14] E. Nazaretski, J. P. Thibodaux, I. Vekhter, L. Civale, J. D. Thompson, and R. Movshovich, Appl. Phys. Lett. **95**, 262502 (2009).

[15] M. Tinkham, *Introduction to Superconductivity* (Dover Publications, Mineola, New York, 1996).

[16] T. Shapoval, S. Engel, M. Gründlich, D. Meier, E. Backen, V. Neu, B. Holzapfel, and L. Schultz, Supercond. Sci. Technol. **21**, 105015 (2008).

[17] R. E. Treece, M. S. Osofsky, E. F. Skelton, S. B. Qadri, J. S. Horwitz, and D. B. Chrisey, Phys. Rev. B **51**, 9356 (1995).

[18] T. Shapoval, V. Neu, U. Wolff, R. Hühne, J. Hänisch, E. Backen, B. Holzapfel, and L. Schultz, Physica C **460**, 732 (2007).

[19] H. J. Hug *et al.*, J. Appl. Phys. **83**, 5609 (1998).

[20]S. Vock, F. Wolny, T. Mühl, R. Kaltofen, L. Schultz, B. Büchner, C. Hassel, L. Lindner, and V. Neu, Appl. Phys. Lett. **97**, 252505 (2010).
[21]G. Carneiro and E. H. Brandt, Phys. Rev. B **61**, 6370 (2000).
[22]T. R. Albrecht, P. Grutter, D. Horne, and D. Rugar, J. Appl. Phys. **69**, 668 (1991).
[23]A. Wadas and H. J. Hug, J. Appl. Phys. **72**, 203 (1992).
[24]D. S. Inosov *et al.*, Phys. Rev. B **81**, 014513 (2010).
[25]D. V. Evtushinsky *et al.*, New J. Phys. **11**, 055069 (2009); R. Khasanov *et al.*, Phys. Rev. Lett. **102**, 187005 (2009); D. S. Inosov *et al.*, *ibid.* **104**, 187001 (2010).
[26]A. Kamlapure, M. Mondal, M. Chand, A. Mishra, J. Jesudasan, V. Bagwe, L. Benfatto, V. Tripathi, and P. Raychaudhuri, Appl. Phys. Lett. **96**, 072509 (2010).
[27]B. Komiyama, Z. Wang, and M. Tonouchi, Appl. Phys. Lett. **68**, 562 (1996); Z. Wang, A. Kawakami, Y. Uzawa, and B. Komiyama, J. Appl. Phys. **79**, 7837 (1996).
[28]In our temperature range, the changes of $\max(F_{\mathrm{lat}})$ due to the temperature variations of λ in Eq. (4) are smaller than the statistical uncertainties of the measured values given in Table I. Therefore, such averaging is justified. In a broader temperature range, fitting the measured values to Eq. (4) might be necessary.
[29]L. Luan, O. M. Auslaender, T. M. Lippman, C. W. Hicks, B. Kalisky, J.-H. Chu, J. G. Analytis, I. R. Fisher, J. R. Kirtley, and K. A. Moler, Phys. Rev. B **81**, 100501 (2010); Phys. Rev. Lett. **106**, 067001 (2011).
[30]J. Lohau, S. Kirsch, A. Carl, G. Dumpich, and E. F. Wassermann, J. Appl. Phys. **86**, 3410 (1999); S. McVitie, R. P. Ferrier, J. Scott, G. S. White, and A. Gallagher, *ibid.* **89**, 3656 (2001); Th. Kebe and A. Carl, *ibid.* **95**, 775 (2004).
[31]F. Gross, B. S. Chandrasekhar, D. Einzel, K. Andres, P. J. Hirschfeld, H. R. Ott, J. Beuers, Z. Fisk, and J. L. Smith, Z. Phys. B **64**, 175 (1986).
[32]J. Bardeen, L. N. Cooper, and J. R. Schrieffer, Phys. Rev. **108**, 1175 (1957).
[33]D. S. Inosov, J. T. Park, A. Charnukha, Yuan Li, A. V. Boris, B. Keimer, and V. Hinkov (accepted for publication in Phys. Rev. B), e-print arXiv:1012.4041.